Liquid Crystals
Publication details, including instructions for authors and subscription information:
http://www.informaworld.com/smpp/title~content=t713926090

Molecular modelling of the structures of liquid crystals based on phenyl ester mesogens in the smectic phase

Kuei-Jen Lee

Online publication date: 06 August 2010

To cite this Article Lee, Kuei-Jen(1998) 'Molecular modelling of the structures of liquid crystals based on phenyl ester mesogens in the smectic phase', Liquid Crystals, 25: 6, 661 — 678
To link to this Article: DOI: 10.1080/026782998205688
URL: http://dx.doi.org/10.1080/026782998205688

LIQUID CRYSTALS, 1998, VOL. 25, NO. 6, 661–678

Molecular modelling of the structures of liquid crystals based on phenyl ester mesogens in the smectic phase

KUEI-JEN LEE
Deh Yu College of Nursing and Management, Keelung, Taiwan 203, ROC

GING-HO HSIUE*, JUNG-LUNG WU and JR-HONG CHEN
Department of Chemical Engineering, National Tsing Hua University, Hsinchu, Taiwan 30043, ROC

(*Received 22 November 1995; accepted 17 April 1998*)

In this work, an atom-based molecular modelling technique is applied to determine the structures of smectic E, A, and C phases composed of phenyl ester mesogens. These mesogenic molecules are abbreviated as MD*n*21B. A computer search with molecular mechanics calculations is performed to identify the possible low energy configurations of two adjacent molecules. According to these results, the isolated molecules with their optimized structures approach dimer associations, and the favourable alignments are antiparallel. Depending on the lowest energy associations, ten different initial models for each phase, to simulate X-ray diffraction patterns, are developed by packing the dimers with an antiparallel association into periodic boxes. Also, relaxed models are obtained by applying cycles of energy minimization and molecular dynamics under (NVT) conditions at 500 K to these initial models. Molecular dynamics runs under (NPT) conditions are then performed on these relaxed models at a temperature of each smectic phase chosen to approach equilibrated structures in these phases. Simulations are also performed, and detailed molecular structures analysed, on the basis of these equilibrated structures. The simulated X-ray diffraction patterns for smectics E, A, and C are in good agreement with those obtained experimentally. The distributions of the dihedral angles at the bonds in the aromatic cores indicate that more fluctuations occur in the smectic A and C phases than in the smectic E. The average values of the aromatic core overlap, as calculated between neighbouring mesogens in the smectic phases, are in the range 4.78–5.91 Å. These values are slightly higher than those found in experimental X-ray diffraction patterns at the position $2\theta \sim 20^{\circ}$. Total pair correlation functions have a similar appearance for smectics E and A. Also, these pair correlation functions are similar to the results for amorphous polymers, i.e. the total pair correlation functions lose their order outside a spherical shell with radius γ greater than 5 Å.

1. Introduction

Smectic liquid crystals [1] have attracted much interest owing to their unique molecular assembly and electro-optical applications. Previous studies of thermotropic liquid crystals have revealed a variety of smectic phases [2], e.g. smectics A, B, C, E, F, G, and H. These phases vary in their layer structures and tilt angles, and are characterized by both orientational and positional orders. Smectics B, E, F, G, and H are crystalline and have a well defined crystallographic structure within a layer. In the smectic A (SmA) phase, the molecules within a layer are parallel to each other and the long axes are perpendicular to the layer plane. In the smectic C (SmC) phase, the molecules are tilted by an angle with respect to the layer normal. Both smectics A and C have liquid-like layers in two dimensions and a uni-dimensional crystal order. Another range of smectic mesophases which have been thoroughly investigated are the chiral smectic C (SmC*) liquid crystals. Meyer *et al.* [3] first discovered ferroelectricity in SmC* systems, many of which have found extensive applications in display devices, waveguide switching, and optical computing [4]. In the SmC* phase, similar to the SmC phase, the molecules are tilted by an angle relative to the layer normal and form a helical structure by rotating successive layers at a certain angle with respect to the preceding layer. A SmC phase belongs to a C_{2h} symmetry, which is reduced to C_2 [5] when the SmC phase is formed by chiral molecules. On the other hand, a SmA phase is composed of chiral molecules, implying that the SmA phase with a $D_{\infty h}$ symmetry is reduced to D_{∞} [6].

*Author for correspondence.

0267–8292/98 $12.00

The molecular structures of liquid crystals are important since these structures determine their intermolecular interactions and relative orientations. The molecular assembly of a smectic mesophase is based on the intermolecular interactions within each smectic layer; these interactions play an essential role in various kinds of liquid crystalline phase transition. X-ray diffraction patterns can provide valuable information regarding (a) the smectic layers corresponding to a sharp Bragg reflection at small angles and (b) the lateral packing associated with a broad reflection at wide angles. To our knowledge, however, molecular structures and intermolecular interactions remain unclear, since it is extremely difficult to obtain this microscopic information by experimental methods. Attempts to probe these problems have stimulated our use of computer simulations in this study. Two possible configurations are available for two mesogenic molecules: one alignment is parallel, and the other is antiparallel, depending on their intermolecular interactions. If mesogenic molecules possess strongly polar chemical groups, e.g. –CN or $-NO_2$, these mesogens have a tendency to form dimers [7], and exhibit a preference for antiparallel association [8] owing to polar interactions. Simulations and theoretical approaches [9–12] have addressed this problem more thoroughly to understand dimer associations. For example, the smectic A_d phase has a partial bilayer structure with a layer spacing $d \approx 1.5l$, where l is the molecular length. This phase is usually composed of antiparallel dimers, which are due to the existence of permanent electric dipoles. Another example is that the smectic phase with A_1 structure could be formed either by antiparallel dimers or by parallel dimers with a layer spacing $d \approx l$.

Our previous studies [13–15] have extensively studied ferroelectric liquid crystals containing oligo-oxyethylene spacers, various chiral moieties, and two or three aromatic rings of ester core units. In this study, we concentrate on the mesogenic molecules that were studied experimentally in the preceding paper [16]. More specifically this study attempts, via a computer search [17] which has been used to study cholesterol–cholesterol intermolecular interactions, to find the favourable associations of two mesogenic molecules which are in optimized structures. Also, the corresponding interaction energies are calculated according to van der Waals and Coulombic interactions. On searching, dimers that are formed at the lowest interaction energy are selected for packing initial models with periodic boundary conditions for simulations. The purpose of this work is to study the bulk structures of smectics E, A, and C by using atom-based molecular modelling. Simulations are performed on the equilibrated models to obtain X-ray diffraction patterns, the d spacings of the smectic layers, and the pair correlation functions. Moreover, since the simulated models are constructed at an atomistic level, these model systems can provide us with detailed information not only on the intramolecular structures, demonstrated by dihedral angles, but also on the intermolecular features, which are described by the aromatic core overlap.

2. Simulations

2.1. *Dimer search*

Figure 1 represents the chemical formulae of MDn21B ($n = 1, 2$) as used in these simulations. An MD121B molecule contains 77 atoms with hydrogen atoms included, and an MD221B molecule contains 84 atoms. The interactions of two adjacent molecules of MDn21B that are in optimized structures were used to search for possible low energy associations. The coordinate system of the two molecules was rotated by each molecule through three Euler angles ϕ, θ, and ψ. The matrix $\boldsymbol{A}$ corresponding to a rotation through the three Euler angles is formulated as [18]

$$\boldsymbol{A} = \begin{bmatrix} \cos\psi\cos\phi - \cos\theta\sin\phi\sin\psi & \cos\psi\sin\phi + \cos\theta\cos\phi\sin\psi & \sin\psi\sin\theta \\ -\sin\psi\cos\phi - \cos\theta\sin\phi\cos\psi & -\sin\psi\sin\phi + \cos\theta\cos\phi\cos\psi & \cos\psi\sin\theta \\ \sin\theta\sin\phi & -\sin\theta\cos\phi & \cos\theta \end{bmatrix}. \quad (1)$$

Thus, the relative orientation of two adjacent molecules can be defined by six degrees of freedom. However, the search algorithm [17] was designed for two of the six axes to coincide. Therefore, this operation was performed on a search of five degrees of freedom. Angles lying between 0° and 360° at equal intervals of 30° were chosen for the three Euler angles. This search produced 248 832 (12^5) configurations. The energies of these configurations were computed and the lowest 400 were

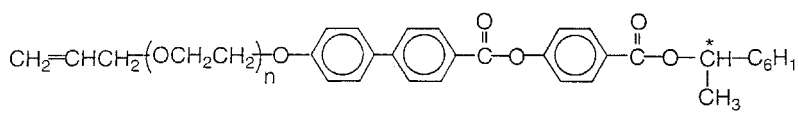

Figure 1. Chemical/structural formula for MDn21B.

chosen for further analysis. The intermolecular interactions of these configurations were calculated according to van der Waals and Coulombic interactions. The intermolecular interactions between atomic pairs are described by 12-6 Lennard–Jones potential

$$E_{ij} = \varepsilon_{ij}\left[\left(\frac{r^{o}_{ij}}{r_{ij}}\right)^{12} - 2\left(\frac{r^{o}_{ij}}{r_{ij}}\right)^{6}\right] \quad (2)$$

where ε_{ij} is the well depth in kcal mol^{-1}, r^{o}_{ij} is the interatomic distance in Å at which the minimum energy can be obtained, and r_{ij} indicates the distance between atoms i and j. Heteronuclear interactions for ε_{ij} and r^{o}_{ij} are computed as geometric averages. They are given as

$$\varepsilon_{ij} = (\varepsilon_{ii}\varepsilon_{jj})^{1/2} \quad (3)$$

and

$$r^{o}_{ij} = (r^{o}_{ii}r^{o}_{jj})^{1/2}. \quad (4)$$

The van der Waals parameters, as used in equation (2), were taken from the Dreiding II force field [19]. The electrostatic interactions between the partial charges of the atoms within the two molecules were calculated with the function

$$E_{\mathrm{Coul}} = C_0 q_i q_j/(\varepsilon r_{ij}) \quad (5)$$

where q_i and q_j are the charges in electron units, r_{ij} is the distance in Å, ε is the dielectric constant, and E_{Coul} is in kcal mol^{-1} when $C_0 = 332.06$. Partial atomic charges used in equation (5) were assigned by charge-equilibration calculations [20], as provided in Cerius^2 supplied by Molecular Simulations, Inc. [21].

2.2. *Molecules packed in the simulated cells*

The resulting dimers with the lowest energy configurations were used to construct simulation models for smectics E, A, and C. Preliminary simulations were carried out on MD121B packed in simulated cells with seven and eight molecules to study the initial phase behaviour of the smectics E and A, respectively. A smectic E (SmE) model, which is hexagonal with two molecules in a crystal unit cell, was packed according to Doucet and coworkers [22]. A SmA model was first constructed with a crystal model containing eight molecules (four dimers) through the crystal builder using a space group $P1$ in Cerius^2. These molecules were thus confined in a simulated cell. Subsequently, the molecular coordinates in the simulated cell were randomly transferred in the directions of the A- and B-axes, based on computer-generated random numbers. On the other hand, the coordinates in the direction of the C-axis were maintained in a crystal order. In this way an initial SmA model could be constructed. Following the initial study, simulations were carried out on expanded models. Ten starting models were constructed for smectics E, A, and C. Each initial model containing 12 molecules (6 dimers) was used to simulate the SmE phase. Since, in future work, we will extend these models to allow simulation of side-chain liquid crystalline polymers by incorporating a backbone with a degree of polymerization of 35, each initial model containing 36 molecules (18 dimers) was constructed for the SmA phase. In addition, the molecules in the initial SmA models were then tilted with respect to the normal of the plane that is defined by the A- and B-axes to obtain the initial SmC models.

Several authors [23–25] have recently reported the simulation studies of X-ray diffraction patterns for liquid crystalline systems by using optimized models, which were minimized by molecular mechanics. However, simple energy minimization cannot sufficiently reduce the internal stress of the initial models. Therefore, in this work the initial models were alternately subjected to molecular mechanics and molecular dynamics runs [26–28] to approach the relaxed structures. In the packing process, an intermolecular separation may lead to closest atom–atom distances that are smaller than the sum of the van der Waals radii. Thus, this operation may force the initial models into local minima with high energy states. The initial models were minimized by using steepest descents for 500 steps. To prevent these initial models from becoming trapped in a high energy state, molecular dynamics runs at a temperature of 500 K were performed on them after the initial energy minimization. Molecular dynamics is used to provide the kinetic energy required for conformational motions so that the structures can move out of the local energy minima.

Cycles of energy minimization and molecular dynamics were then performed on the first minimized models with periodic boundary conditions. Here, the minimization method is conjugate-gradients with the cell dimensions optimized. The molecular dynamics was performed under a canonical (NVT) ensemble by the Nosé thermal coupling method [29, 30]. The Dreiding II force field [19], as provided in Cerius^2, was used for the energy calculations. The potential energy of the system, E, was calculated from the following terms:

$$E = E_l + E_\theta + E_\phi + E_{\mathrm{inv}} + E_{\mathrm{vdW}} + E_{\mathrm{Coul}} \quad (6)$$

where E_l, E_θ, E_ϕ are the bond stretching, bond angle bending, and dihedral angle torsion, respectively, E_{inv} is the improper out-of-plane interaction, and E_{vdW} and E_{Coul} are the van der Waals and Coulombic interactions, respectively. All atoms in the mesogenic molecules were assigned with partial charges calculated by using the charge-equilibration algorithm [20] in Cerius^2. The criterion of energy convergence is to obtain a root-mean-square force less than 0.1 kcal mol^{-1} Å^{-1} in the simulated systems. Each cycle of energy minimization

continued until convergence of the energy took place. In molecular dynamics runs, the time step, $\delta t = 1.0$ fs, was used to integrate the Nosé equation of motion by a leap-frog Verlet algorithm [31]. The length of a molecular dynamics run was 20 ps. Ten to fifteen cycles of energy minimization and molecular dynamics were usually carried out on each model structure. When the structures of the models become too well relaxed, further molecular dynamics runs were performed under an isobaric-isothermal (NPT) ensemble at a temperature for each smectic phase and 1 atm for a duration of 200–300 ps for the well relaxed models, to ensure that the systems approach equilibration in the smectic phase. However, preliminary simulations with small simulated cells were performed under (NPT) conditions for longer runs (500 ps). Moreover, X-ray diffraction patterns were simulated by averaging the ten equilibrated structures for each smectic state. Diffraction patterns for powders were simulated by using the Diffraction Crystal module in Cerius[2]; these results are compared with those obtained experimentally [16]. All measurements for each smectic phase were based on the ten equilibrated configurations in which the corrections of the structures had been verified by the simulated X-ray diffraction patterns. These simulations were run on an IRIS Indigo[2] Impact 10,000 computer.

3. Results and discussion

3.1. *Dimer associations*

As indicated in figure 1, the chemical structures have (*R*)- and (*S*)-forms of their absolute configurations about the chiral centre (C*). Since experimental results [16] are available for the (*R*)-form, molecules of (*R*)-MD*n*21B were simulated for comparison in this study. The geometry of the monomers (figure 1) was optimized in vacuum by molecular mechanics using the Dreiding II force field [19] in Cerius[2]. For comparison, the optimized monomers were then calculated with the aid of AM1 [32], which is available in MOPAC 6.0 [33]. Here, the reported results were primarily focused on the aromatic core. Figure 2 shows the aromatic core of MD*n*21B in which the dihedral angles are noted as ϕ_1 through ϕ_5. Results obtained from dihedral angles at the optimized state for ϕ_1 through ϕ_5 are $\sim\pm41°(\sim\pm40°)$, $\sim\pm168°(\sim\pm175°)$, $\sim\pm176°(\sim\pm178°)$, $\sim\pm27°(\sim\pm40°)$, and $\sim\pm176°(\sim\pm179°)$, respectively.

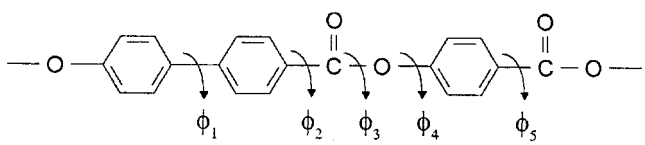

Figure 2. Definition of dihedral angles at bonds in the aromatic core.

Here, the values in parentheses were calculated according to AM1. There are a few values that are inconsistent between the Dreiding II force field and the AM1 calculations; high values of discrepancy can be identified for ϕ_2 and ϕ_4. Except for ϕ_1, The AM1 calculations give higher values of dihedral angles than those calculated with the Dreiding II force field. Based on these calculations, two favourable conformations can be identified from the dihedral angles at the bonds in the aromatic core of an isolated molecule: one is near the region of the *cis* conformation, such as ϕ_1 and ϕ_4, and the other is the *trans* conformation, such as ϕ_2, ϕ_3, and ϕ_5.

The molecules of MD*n*21B at their optimized structures from the Dreiding II force field were treated as rigid rods in the computer search procedure. The intermolecular interactions were calculated according to the atomic pairs from only two different molecules; the pairwise interactions were calculated according to equations (2) and (5). In these calculations, the dielectric constant $\varepsilon = 1$ was used in equation (5). The lowest 400 of the total number of computer searches were printed out for analysis. Table 1 summarizes the ten lowest energy dimers of the 400 searched configurations for MD*n*21B.

Figures 3 (*a*) and 3 (*b*) show two snapshots for MD121B, corresponding to the lowest energy configurations, for the antiparallel dimer (-21.03 kcal mol^{-1}) and for the parallel dimer (-18.85 kcal mol^{-1}), respectively. Two structures with the lowest interaction energies for MD221B similar to those shown in figure 3 are the antiparallel (-22.74 kcal mol^{-1}) and parallel (-18.99 kcal mol^{-1}) dimers. Other dimers shown in table 1 have structures that are slightly perturbed from the antiparallel or parallel dimers of the lowest energy configurations along

Table 1. Ten lowest interaction energies for the dimer associations of MD*n*21B.

Molecule	Antiparallel[a]	d_1/Å[b]	Parallel[a]	d_2/Å[c]	l/Å[d]
MD121B	−21.03	34.15	−18.85	34.10	31.90
	−20.11	35.29	−17.86	34.70	
	−19.83	33.10	−17.06	33.98	
	−19.31	34.00	−16.81	33.77	
	−19.09	33.00	−16.57	32.78	
MD221B	−22.74	40.44	−18.99	37.00	35.27
	−21.21	39.90	−17.55	36.10	
	−19.83	36.44	−17.22	36.50	
	−19.49	37.32	−16.81	37.90	
	−18.85	37.30	−16.51	36.40	

[a] Intermolecular interactions (in kcal mol^{-1}) calculated according to equations (2) and (5).
[b] Dimer lengths for antiparallel associations.
[c] Dimer lengths for parallel associations.
[d] Monomer length based on the structure optimized by the Dreiding II force field.

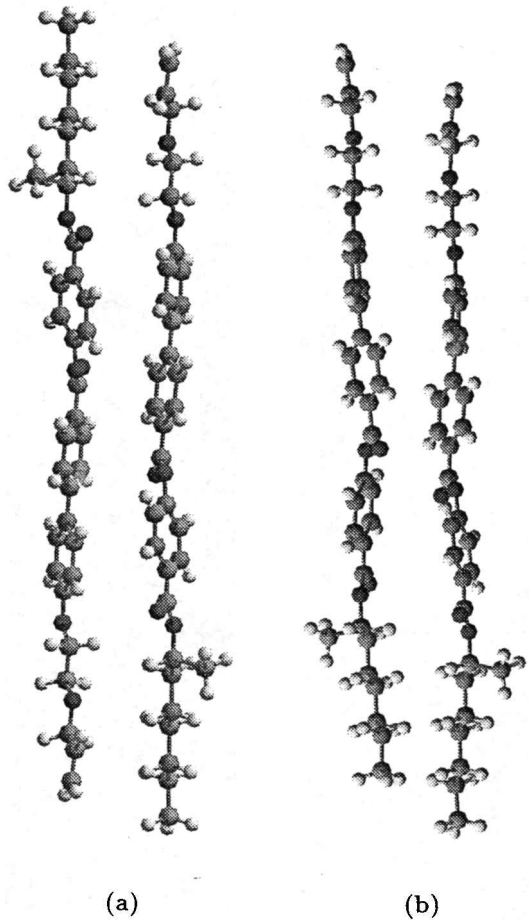

Figure 3. The lowest energy configurations of the antiparallel and parallel associations: (*a*) antiparallel dimer, (*b*) parallel dimer.

the molecular long axis, thereby causing the dimer length to be slightly different in each dimer association. As shown in table 1, the average energy gaps between the antiparallel and parallel dimers are 2.44 kcal mol^{-1} for MD121B and 3.01 kcal mol^{-1} for MD221B; these energy gaps are favourable for antiparallel associations. Table 1 also indicates that two distinct antiparallel associations, significantly lower in energy than any other dimers, can be identified as -21.03 kcal mol^{-1} for MD121B and -22.74 kcal mol for MD221B, these dimers with the lowest energy associations were packed into the simulated cells for simulations.

3.2. *Equilibration of systems*

Equilibrated structures can be obtained by performing further molecular dynamics runs under (NPT) conditions at the temperatures, as shown in table 2 on the well relaxed structures. The structures of these smectic phases are usually determined by X-ray diffraction patterns in which *d* spacings and lateral spacings can be measured. Since *d* spacings and lateral spacings are dependent on volume variation, the fluctuations of the volumes of the systems due to molecular dynamics runs were observed during equilibration. Equilibration was determined by the time at which the dynamics of the volumes fluctuated symmetrically with respect to their most probable values.

For preliminary studies, molecular dynamics runs were performed for 500 ps on the cells of seven and eight MD121B molecules for the SmE and SmA phases, respectively. As shown in table 2, runs were carried out at 323 K for the SmE phase and at 393 K for the SmA phase. Figures 4 (*a*) and 4 (*b*) display the fluctuations of the volumes as a function of time for the SmE phase and for the SmA phase, respectively. It is readily apparent that the approaching equilibration for the SmE model is faster than that for the SmA model. The SmE phase system obtains its equilibration after 40 ps, while the SmA phase system obtains its equilibration after 280 ps.

Following the preliminary studies, simulations were performed on expanded samples that are cells of 12 MD*n*21B ($n=1,2$) molecules for the SmE phase, of 36 MD*n*21B ($n=1,2$) molecules for the SmA phase, and of 36 MD221B molecules for the SmC phase. For the smectics E, A, and C, ten configurations were constructed for each phase, all with well relaxed structures.

Table 2. Unit cell dimensions[a], temperature, and density of the equilibrated systems for MD*n*21B.

n	Phase	*a*	*b*	*c*	T[b]	ρ[c]
1	SmE	15.98 ± 0.09	16.39 ± 0.11	34.55 ± 0.23	323	1.17 ± 0.01
1	SmA	31.28 ± 0.31	31.31 ± 0.36	34.01 ± 0.15	393	0.95 ± 0.02
2	SmE	16.95 ± 0.02	16.32 ± 0.10	36.74 ± 0.18	300	1.13 ± 0.01
2	SmA	32.10 ± 0.17	30.84 ± 0.25	34.88 ± 0.21	363	0.99 ± 0.01
2	SmC	32.27 ± 0.15	30.68 ± 0.06	34.46 ± 0.12	308	1.01 ± 0.01

[a] Unit cell dimensions (in Å) represented as *a*, *b*, and *c*.
[b] The temperature (in K) at which further molecular dynamics runs were performed. These temperatures were obtained from previous work [16].
[c] Density of the equilibrated systems (in g cm^{-3}).

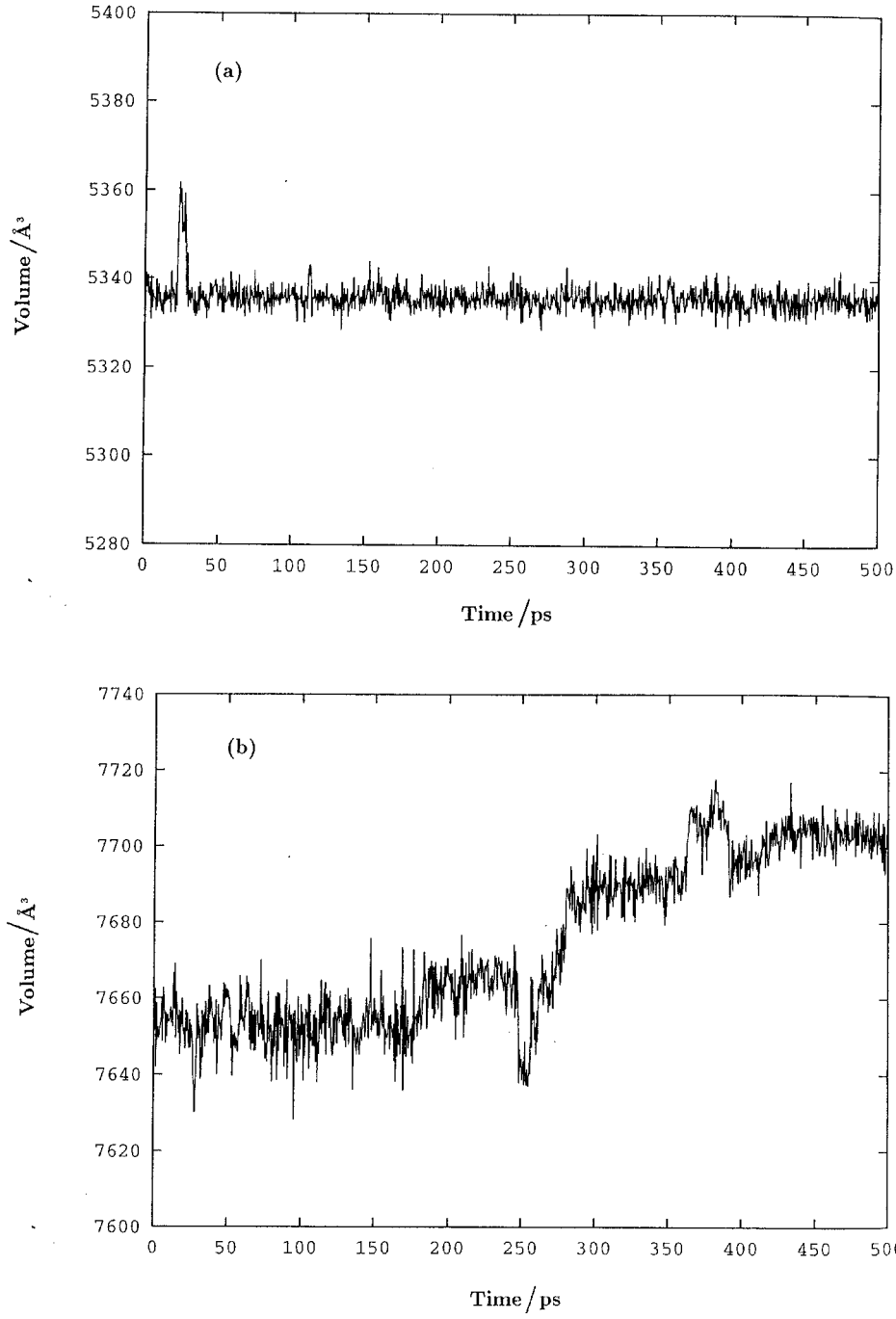

Figure 4. Fluctuations of volume with time for the small systems composed of MD121B: (*a*) in the SmE phase at 323 K, (*b*) in the SmA phase at 393 K.

To determine the time when the phases gain their equilibration, molecular dynamics runs (NPT) were first carried out for 300 ps on one of the ten relaxed samples packed with MD121B molecules, at 323 K and 393 K for the SmE and SmA phases, respectively, and one packed with MD221B molecules for the SmC phase at 308 K. Figures 5 (*a*), 5 (*b*), and 5 (*c*) show the flunctuations of the volumes of these systems with time for smectics E, A, and C, respectively. The total amount of time allowed for equilibration can be identified as 40 ps for the SmE phase, 120 ps for the SmA phase, and 110 ps for the SmC phase. Figures 4 (*a*) and 5 (*a*) indicate that the systems of the SmE phase obtain their equilibration after the same time, independently of the size of the simulated cells. On the other hand, as figures 4 (*b*) and 5 (*b*) show, it is interesting to find that the approaching equilibration of the larger size is faster than that of the smaller. Therefore production runs were performed on the larger systems for each phase. Following these equilibration runs, molecular dynamics runs (NPT) were

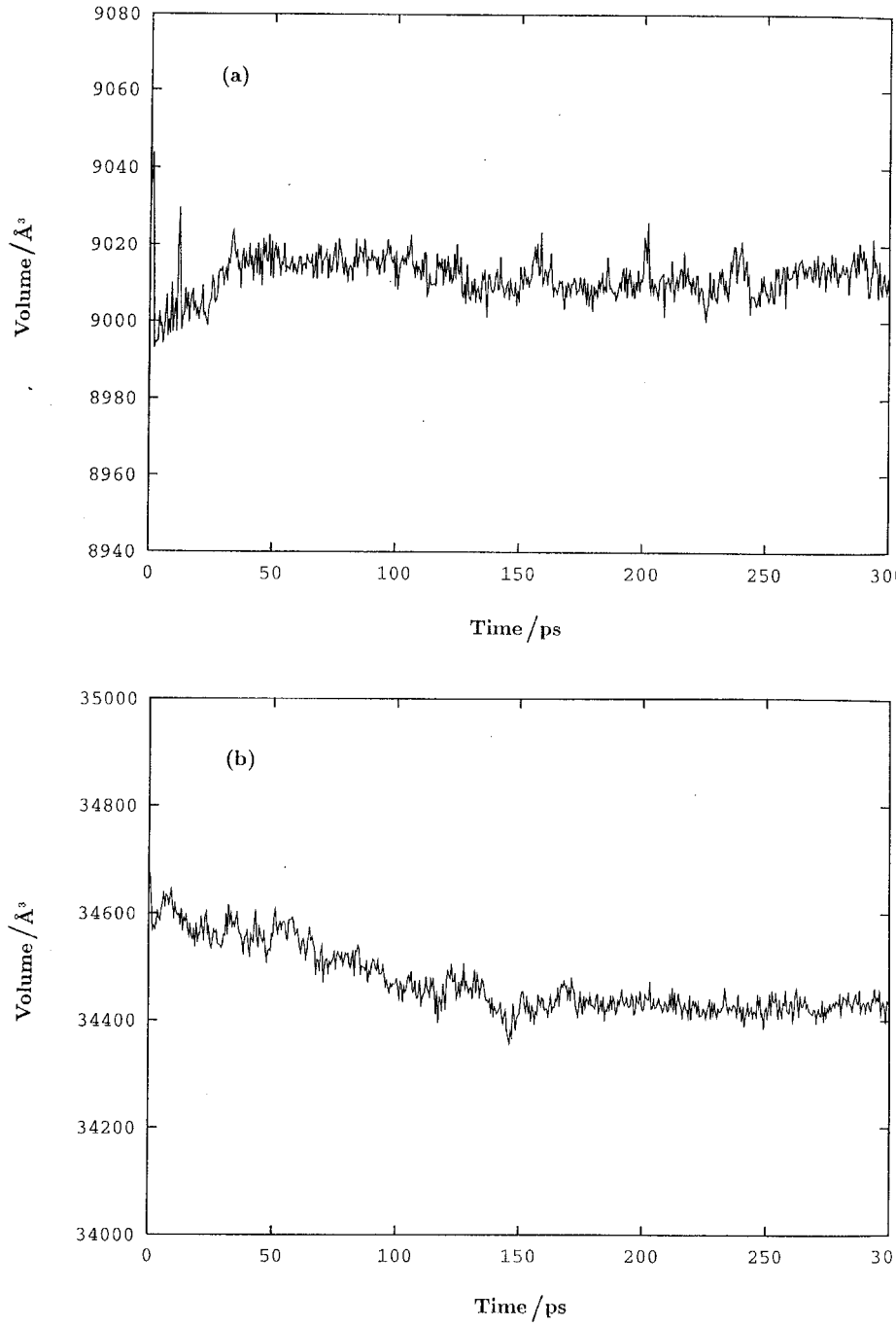

Figure 5. Fluctuations of volume with time for the expanded systems. The systems for the SmE and SmA phases are composed of MD121B, and that for the SmC of MD221B. (*a*) SmE phase at 323 K, (*b*) SmA phase at 393 K, (*c*) SmC phase at 308 K.

performed on the rest of the well relaxed expanded systems for 200 ps at the temperatures shown in table 2, to equilibrate these systems for each smectic phase.

Table 2 also summarizes the unit cell dimensions and densities of the equilibrated systems. Values of the dimensions were obtained by averaging the ten equilibrated structures of each phase. Averaged densities have standard deviations between 0.01 and 0.02.

3.3. *Simulations of X-ray diffraction patterns*

Simulations of X-ray diffraction patterns were focused primarily on the smectics E, A, and C; the simulations were performed on already equilibrated structures. Figure 6 presents one of the ten equilibrated models of the simulated SmE phase. The initial model in this figure, constructed according to the proposal of Doucet and coworkers [22], was packed with six dimers of

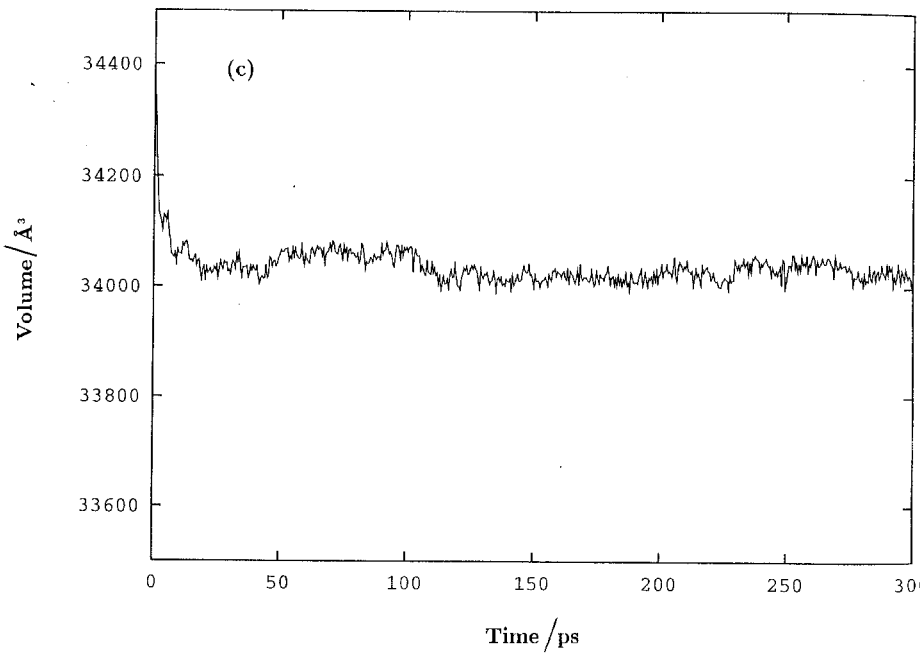

Figure 5. (*continued*).

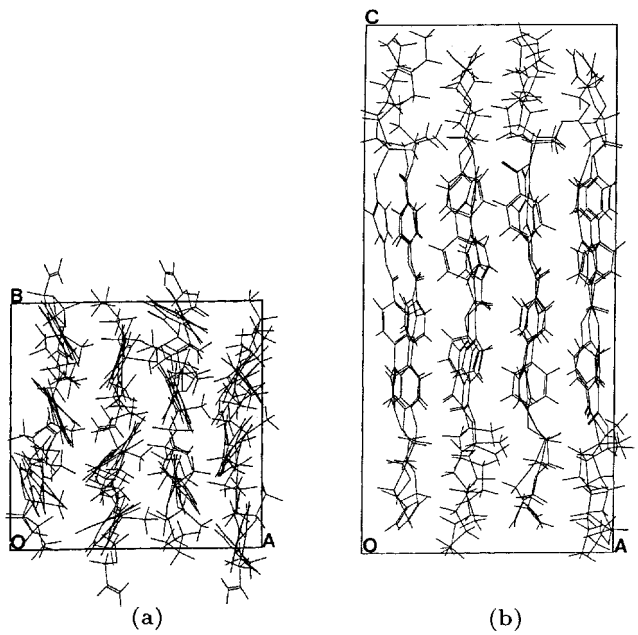

Figure 6. An equilibrated SmE model shown in a periodic unit cell: (*a*) view along the C-axis, (*b*) view along the B-axis.

MD121B with antiparallel association. Figure 7(*a*) displays the simulation and experimental results of X-ray diffraction patterns. The solid line in figure 7(*a*) shows the resulting simulations of X-ray diffraction patterns, based on the equilibrated models; the broken line is an experimental result obtained from our previous work [16]. As indicated in figure 7(*a*), these two curves closely correspond to each other. Simulations were also performed on equilibrated models that were packed with six dimers of MD221B with antiparallel association. The solid line in figure 7(*b*) shows the simulation results of the X-ray diffraction patterns; a comparison was made by extracting X-ray diffraction patterns from figure 4 of our previous work [16] (broken line). Comparison of these two curves in figure 7(*b*) reveals an agreement between the main peaks indexed by 1 1 0, 1 1 1, and 2 0 1. Two shoulders beside the main peaks appear in the solid line, which may give the indices of 1 1 1 and 2 0 1, respectively. As shown in figures 7(*a*) and 7(*b*), the X-ray diffraction patterns of the SmE phase display a sharp Bragg reflection from the smectic layers at small angles. On the other hand, at large diffraction angles, the diffraction patterns are separated; hence the order inside the layers has a crystalline character.

Figure 8 shows one of the ten equilibrated structures of the simulated SmA phase, as constructed from eighteen antiparallel dimers of MD121B. Also, the broken line in figure 9(*a*) shows an experimental X-ray powder diffraction pattern of MD121B extracted from our previous work [16]. Figure 9(*a*) also displays a simulated X-ray powder diffraction pattern (solid line); this pattern was simulated on the basis of the equilibrated models. Comparing the solid and broken lines in figure 9(*a*) clearly indicates that the simulated pattern reproduces the one obtained experimentally. SmA models for MD221B were also constructed in this study by packing eighteen antiparallel dimers into these models. Figure 9(*b*) shows that the experimental and simulated X-ray patterns (broken and solid line, respectively) agree well.

This work also attempts to simulate the ferroelectric SmC* phase. However, owing to limited computer

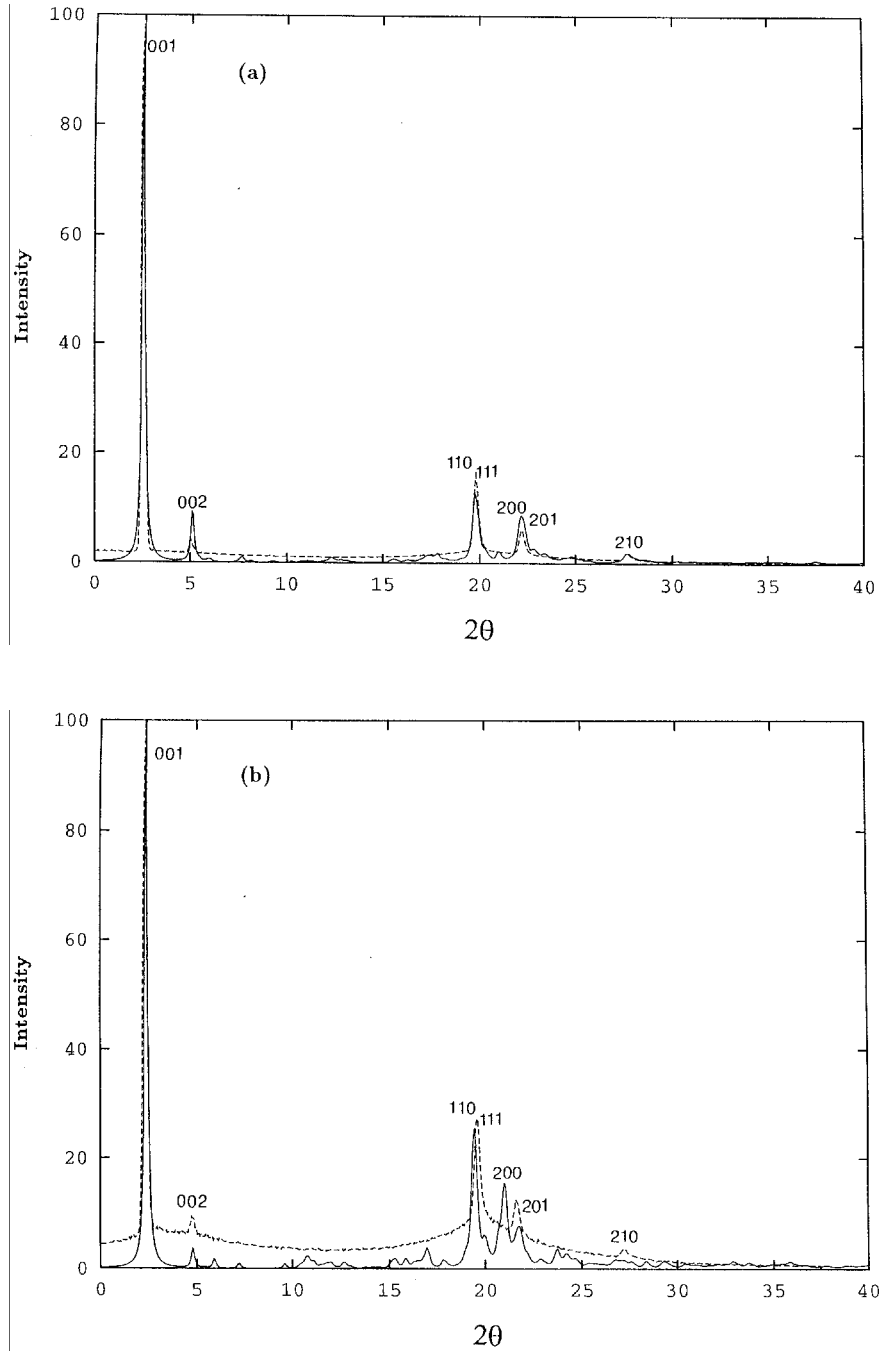

Figure 7. Simulated (solid line) and experimental (broken line) X-ray diffraction patterns of the SmE phase: (*a*) MD121B, (*b*) MD221B.

capacity, simulations can only be performed on the basis of one layer composed of chiral mesogenic molecules. Thus, ten initial models were packed with eighteen antiparallel dimers of MD221B in each periodic cell. Figure 10 shows one of the ten equilibrated structures of the simulated SmC phase, and the averaged tilt angle θ is $8.63^\circ \pm 1.92^\circ$. Simulations of X-ray powder diffraction patterns were performed on these equilibrated models; the solid line in figure 11 shows the resulting pattern. To facilitate a comparison, figure 11 also displays an experimental X-ray powder diffraction pattern of MD221B as a broken line, as obtained from figure 4 of our previous work [16]. The experimental and simulated patterns correspond well. The X-ray diffraction patterns depicted in figures 9 and 11 show a sharp Bragg reflection at small angles corresponding to the smectic layers; in addition, a broad reflection at wide angles is associated with the lateral packing. Moreover, this broad reflection reveals that the order inside the smectic layers is liquid-like in the SmA and SmC phases.

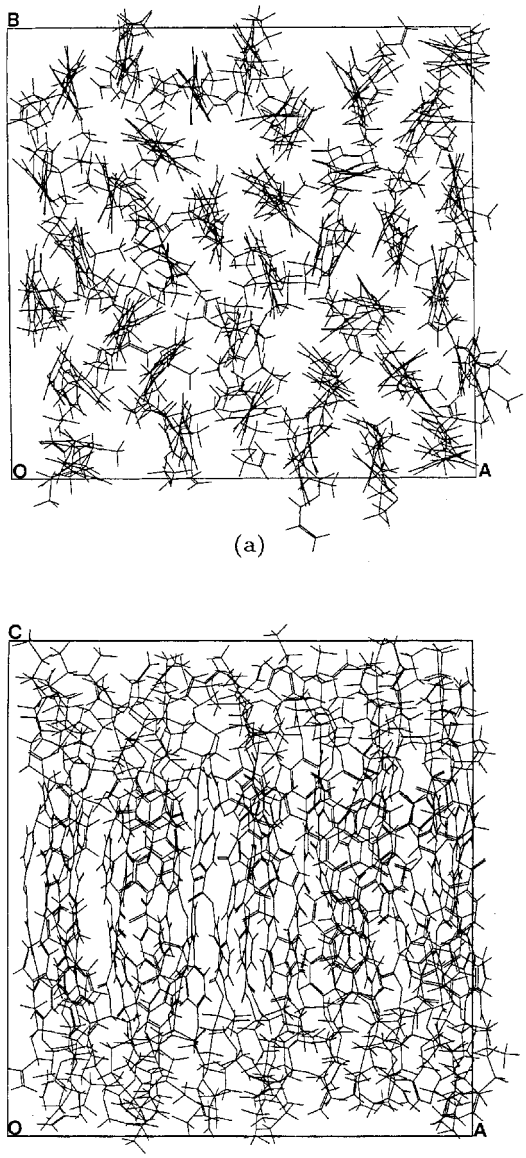

Figure 8. An equilibrated SmA model shown in a periodic unit cell: (*a*) view along the *C*-axis, (*b*) view along the *B*-axis.

3.4. *Distributions of the dihedral angles of the aromatic cores*

Comparing the distributions of the dihedral angles at the bonds in the aromatic cores of the molecules in the bulk with the corresponding dihedral angles of an optimized molecule in vacuum provides a valuable insight into the effects of molecules packed in the simulated systems. Here, the simulated systems that were observed are composed of MD121B for the SmE and SmA phases, and of MD221B for the SmC phase. Figures 12(*a*), 12(*b*), and 12(*c*) show the distributions of the dihedral angles at bonds ϕ_1, ϕ_2, ϕ_3, ϕ_4, and ϕ_5 in the aromatic cores of the molecules in the smectics E, A, and C, respectively. Here, the definitions of ϕ_1 through ϕ_5 are the same as for those in figure 2. In these calculations, the distributions of the dihedral angles were evaluated according to ten equilibrated systems for each phase, i.e. the distribution at each bond in the SmA phase or in the SmC phase was calculated according to 360 dihedral angles, while that at each bond in the SmE phase was calculated with 120 dihedral angles. As shown in figures 12(*a*), 12(*b*), and 12(*c*), by comparing bonds having the same index, the corresponding distributions have a similar appearance. In addition, these figures clearly reveal that the most probable values of the distributions of the dihedral angles can be classified into two regions: one is around the *cis* conformation, such as ϕ_1 and ϕ_4, and the other is centred at the *trans* conformation, such as ϕ_2, ϕ_3, and ϕ_5. This finding correlates well with the results for an isolated molecule, as shown in § 3.1. Furthermore, the dihedral angles at the bonds in the aromatic cores in the SmE, SmA or SmC phases fluctuate about their most probable values; the magnitude, $\delta\phi$, of the fluctuation of a dihedral angle is formulated as

$$\delta\phi = (\langle\phi^2\rangle - \langle\phi\rangle^2)^{1/2} \tag{7}$$

where the angle brackets denote the statistical averages of the enclosed quantity.

Table 3 lists the values of $\langle\phi\rangle$ and $\delta\phi$ for the smectics E, A, and C. A mean value in $\langle\phi\rangle$ denotes the precise location of the most probable appearance of a dihedral angle and a value of $\delta\phi$ represents the breadth of its fluctuations. The distribution curves for ϕ_1 in figures 12(*a*), 12(*b*), and 12(*c*) are split into two regions. The calculations of $\langle\phi\rangle$ and $\delta\phi$ are dependent on these

Table 3. Mean and fluctuation values of the dihedral angles at the bonds in the aromatic core (deg.).

Angle	SmE	SmA	SmC
$\langle\phi_1\rangle^a$	36.1	50.3	65.3
$\delta\phi_1^a$	22.0	29.7	34.3
$\langle\phi_1\rangle^b$	−20.8	−48.2	−45.7
$\delta\phi_1^b$	13.6	28.3	25.8
$\langle\phi_2\rangle$	176.0	178.3	171.5
$\delta\phi_2$	20.5	20.7	25.3
$\langle\phi_3\rangle$	179.0	−177.7	179.4
$\delta\phi_3$	11.0	13.6	14.7
$\langle\phi_4\rangle$	−1.0	2.7	−0.6
$\delta\phi_4$	20.2	29.0	26.6
$\langle\phi_5\rangle$	−178.7	−176.4	−175.1
$\delta\phi_5$	20.3	29.2	32.9

[a] Mean and fluctuation values of the dihedral angle at bond ϕ_1 in the positive region.
[b] Mean and fluctuation values of the dihedral angle at bond ϕ_1 in the negative region.

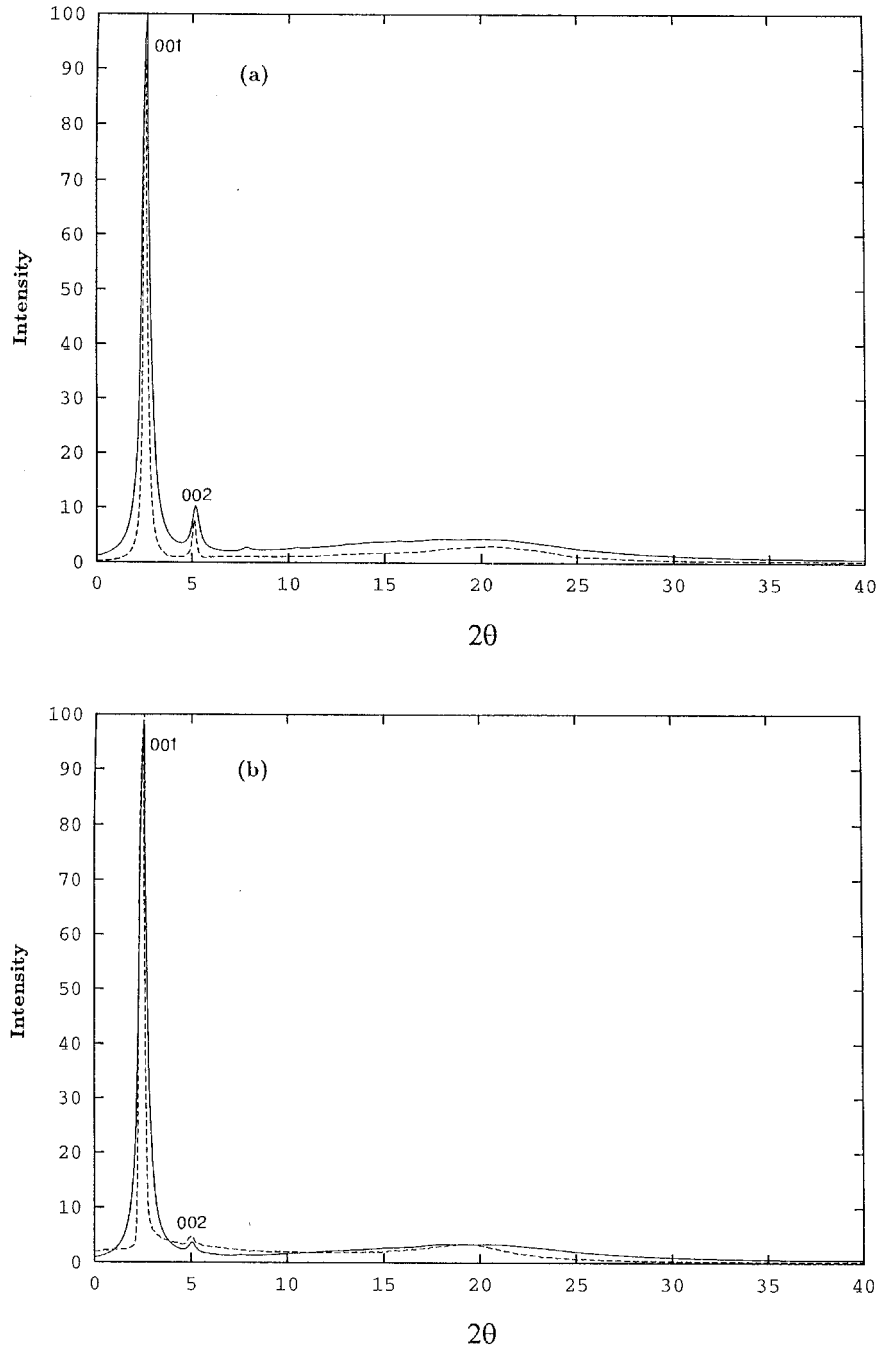

Figure 9. Simulated (solid line) and experimental (broken line) X-ray diffraction patterns of the SmA phase: (*a*) MD121B, (*b*) MD221B.

two regions, and the values of $\langle\phi\rangle$ and $\delta\phi$ are entered into the first four rows of table 3. As shown in table 3, the most probable values of ϕ_1 are $+36.1^\circ$ and -20.8° for the SmE phase, $+50.3^\circ$ and -48.2° for the SmA phase, and $+65.3^\circ$ and -45.7° for the SmC phase. The values of the dihedral angle between the two benzene rings of the biphenyl group have been reported in the range between $\pm30^\circ$ and $\pm65^\circ$ [34–36], by using single crystal X-ray analysis for compounds containing the biphenyl group. Thus the most probable values found for ϕ_1 fall reasonably within this range. On the other hand, the values of $\langle\phi_4\rangle$ are much smaller than those obtained by experimental result, which fall in the range between $\pm55^\circ$ and $\pm57^\circ$ [37, 38]. The most probable values for ϕ_2, ϕ_3, and ϕ_5 correspond well with those found in previous literature [24, 25, 39]. As shown in table 3, the distribution of the dihedral angle at ϕ_3 has the smallest value of $\delta\phi$ in the SmE, SmA or SmC phases because the C–O bond $\langle\phi_3\rangle$ of the ester group has a significant double bond character due to resonance with

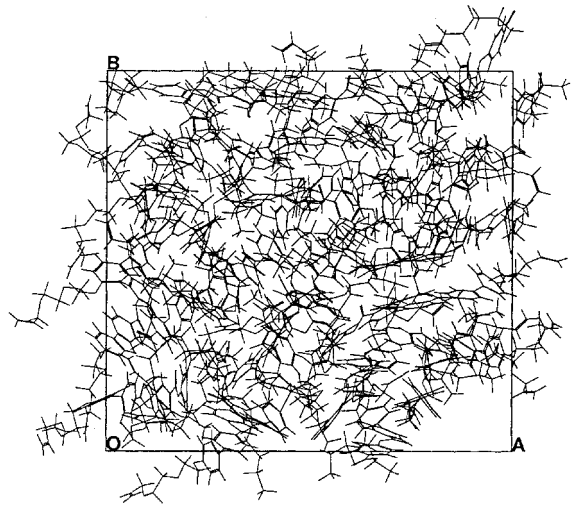

(a)

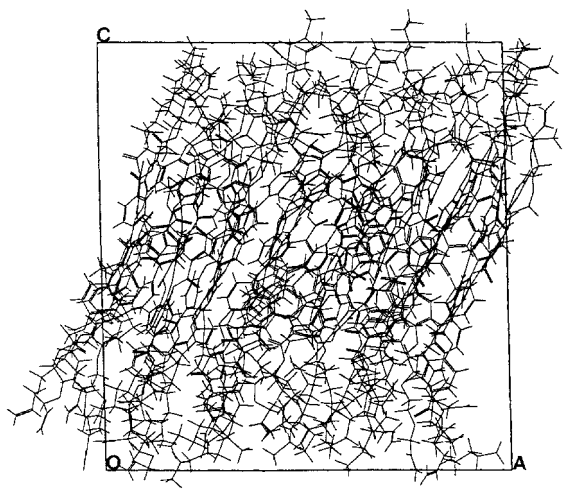

(b)

Figure 10. An equilibrated SmC model shown in a periodic unit cell: (*a*) view along the *C*-axis, (*b*) view along the *B*-axis.

the carbonyl group. In general, the magnitudes of the fluctuations of the dihedral angles in the SmA phase are comparable with those in the SmC phase. However, the values of $\delta\phi$ in the SmE phase are smaller than those in either the SmA or in SmC phases. Therefore, the most probable appearance of the *cis* and *trans* conformations suggests that the Ph–COO–Ph fragment in the molecules is nearly coplanar, thus facilitating favourable intermolecular interactions at the aromatic cores.

3.5. *Calculation of the d spacings*

Table 4 lists the values of *d* spacings obtained for X-ray diffraction patterns at small angles that display a sharp Bragg reflection. These values are denoted parts I and II, respectively, for those obtained from experiment [16] and those obtained from simulations. The values in both parts are in good agreement. The *d* spacings values obtained from equilibrated systems for the smectics E, A, and C, display a systematic trend, i.e. the *d* spacings decrease in the sequence SmE, SmA, SmC. Interestingly, the lengths of the antiparallel dimers of MD121B, as shown in table 1, are comparable with the values of *d* spacings found in the SmE and SmA phases. However, for MD221B, the lengths of the antiparallel dimers, except for 36.44 Å, are slightly greater than the *d* spacings in the SmE, SmA or SmC phase. Crystallization in the SmE phase may force the molecules to be confined in hexagonal lattices, thereby giving the SmE *d* spacings the greatest values. Also, as demonstrated in the previous sections, the order inside the smectic layers is liquid-like in the SmA and SmC phases. Moreover, the dihedral angles in the aromatic cores fluctuate more in the SmA and SmC phases than in the SmE phase. These factors may lead to orientational disorder of the molecular long axis, causing lower *d* spacing values in the SmA and SmC phases than in the SmE phase. Furthermore, the title angle in the SmC phase reduces the *d* spacing in the SmC phase. This may be the reason that the smallest *d* spacing is in the SmC phase.

Table 4. *d* spacings of the smectic phases for MD*n*21B (Å).

	n	SmE	SmA	SmC
I[a]	1	35.56 ± 0.07	34.46 ± 0.13	
	2	36.50 ± 0.20	35.03 ± 0.02	34.87 ± 0.04
II[b]	1	34.58 ± 0.69	33.98 ± 0.64	
	2	36.74 ± 0.78	35.00 ± 0.72	34.64 ± 0.69

[a] Experimental results [16].
[b] Simulation results (this work).

3.6. *Calculation of the aromatic core overlap*

The aromatic core overlap is defined as d_{ij} [40], which is estimated by averaging the distances between the carbonyl groups at molecule *i* and the aromatic rings at the nearest neighbouring molecule *j*, as shown in figure 13. For clarity, figure 13 depicts only the distances that lie between two pairs of carbonyl groups and aromatic rings—other pairs of distances are omitted. The aromatic core overlap was investigated first by using the antiparallel dimer, as shown in figure 3(*a*). This overlap was evaluated from the carbonyl groups at molecule 1 to the aromatic rings at molecule 2. The average values of d_{12} are 5.11 ± 0.80 Å and 5.63 ± 1.28 Å, as estimated according to the five antiparallel dimers in table 1 for MD121B and MD221B, respectively. The aromatic core overlap, d_{ij}, of the smectics E, A, and C

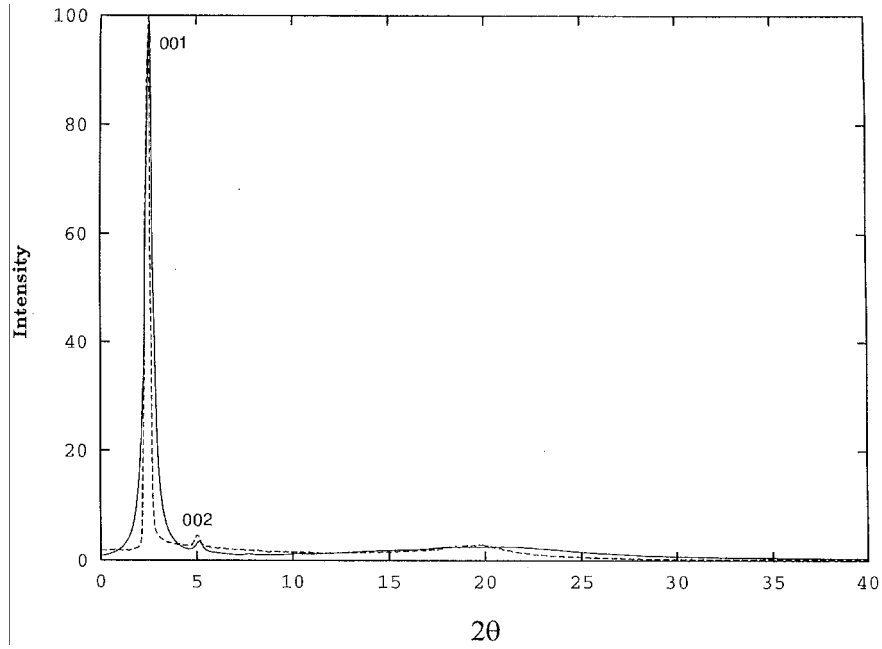

Figure 11. Simulated (solid line) and experimental (broken line) X-ray diffraction patterns of the SmC phase for MD221B.

were evaluated according to their ten equilibrated systems by averaging the distances between the carbonyl groups at mesogen *i* and the aromatic rings at the nearest neighbouring mesogen *j*. The calculated results are summarized in part II of table 5; the values in part I were obtained from experimental results [16], which were evaluated from the broad reflections of X-ray diffraction patterns at wide angles ($2\theta \sim 20°$). As shown in table 5, the values of d_{12} based on dimer associations are comparable with those found in the smectics E, A, and C. In addition, the average values of d_{ij}, as obtained from the core parts of adjacent molecules in the SmE phase, are 4.94 ± 0.85 Å and 5.91 ± 0.99 Å for MD121B and MD221B, respectively. These values correspond to those located near peaks 1 1 0 and 1 1 1, as shown in figures 7 (*a*) and 7 (*b*).

Comparison of the values in part II of table 5 with those shown in part I reveals that the calculated values of d_{ij} are slightly higher than those of the lateral spacings in the smectic phases. This is because intermolecular interactions between the pairs of aromatic cores are slightly shifted along the molecular long axis. This finding suggests that the carbonyl groups at mesogen *i* do not perpendicularly face the aromatic rings at the neighbouring mesogen *j*. From table 5, it is clear that the highest value of d_{ij} for MD221B in the SmE phase causes the highest of *d* spacing value for MD221B in the same phase (see table 4). Moreover, part II of table 5 shows that the average values of the aromatic core overlap fall in the range of 4.78–5.91 Å, and the most probable value of this range can be identified as ~5.2 Å, suggesting that there is a local order at this range [28] due to van der Waals interactions. Furthermore, the average values of d_{ij} for the SmA phase are in the range of 4.78–5.20 Å, which are located close to the position $2\theta \sim 20°$. This finding may support the fact that the 4.5 Å reflection associated with the average lateral packing between aromatic cores is invariably observed in SmA phases [1].

Table 5. Lateral spacings of the smectic phases for MD*n*21B (Å).

	n	SmE	SmA	SmC
I[a]	1	4.52 ± 0.02	4.63 ± 0.05	
	2	4.51 ± 0.01	4.52 ± 0.03	4.46 ± 0.04
II[b]	1	4.94 ± 0.85	5.20 ± 0.99	
	2	5.91 ± 0.99	4.78 ± 1.07	5.23 ± 1.15

[a] Experimental results [16], as obtained at the position $2\theta \sim 20°$.

[b] Calculated values of aromatic core overlap (d_{ij}).

3.7. *Pair correlation functions*

The local structure of a simulated system is described by the pair correlation function. The pair correlation function is calculated as the statistical relationship of a given atom *i*, positioned at a certain point in the simulated system, with the number of atoms in a spherical cell of radius *r* and thickness Δr around atom *i*. The relation [31] is formulated as

$$g(r) = \frac{\langle n(r) \rangle}{4\pi r^2 \Delta r \rho} \tag{8}$$

where $\langle n(r) \rangle$ is the average number of pairs in a spherical shell located between *r* and Δr, and ρ is the bulk density.

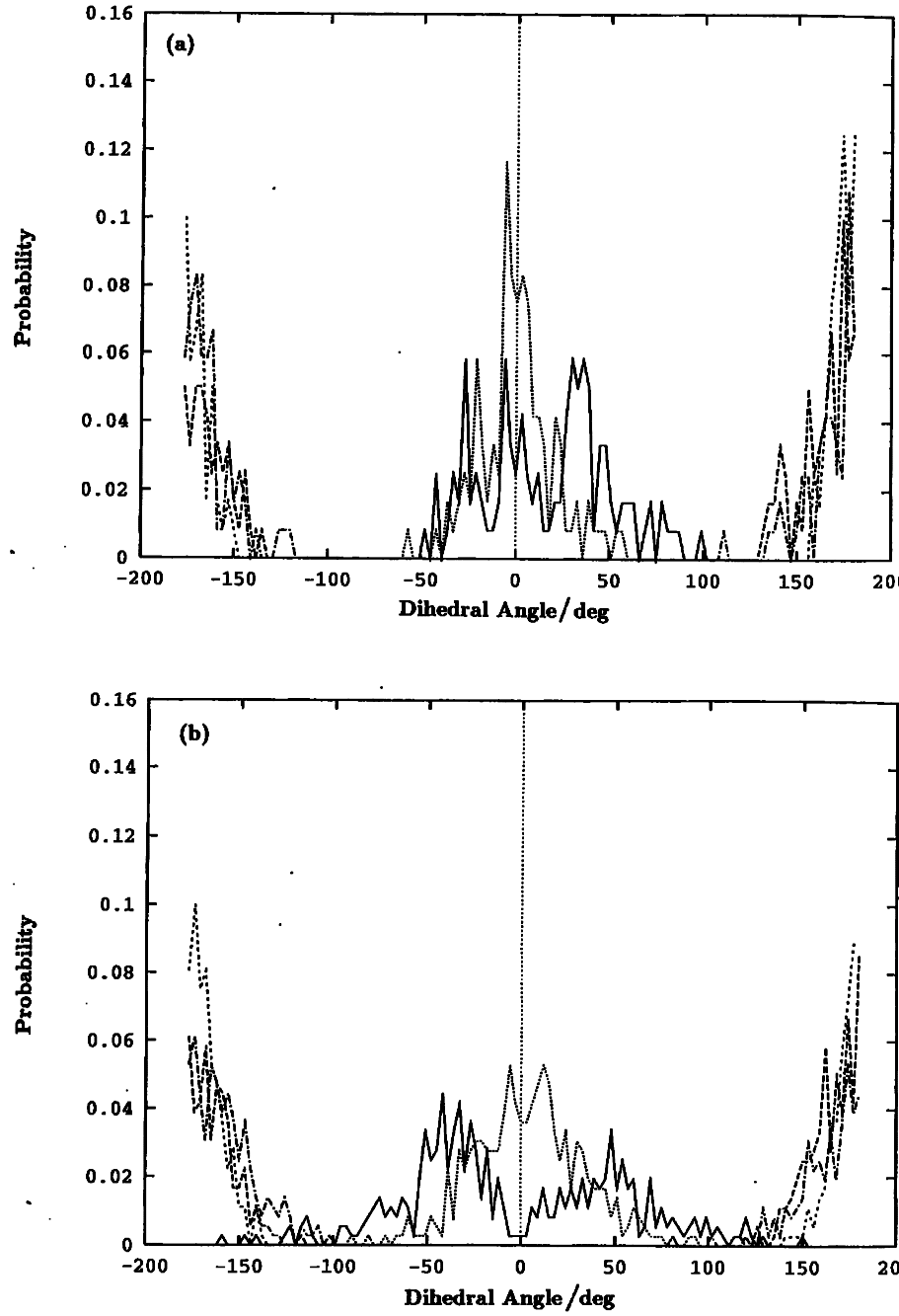

Figure 12. Distributions of the dihedral angles in the aromatic core of MD121B for the bonds indexed by ϕ_1 (solid line), ϕ_2 (line with long dashes), ϕ_3 (line with short dashes), ϕ_4 (line with dots), and ϕ_5 (line with long dashes and dots). (*a*) SmE phase, (*b*) SmA phase, and (*c*) SmC phase.

In reporting the results, $\Delta r = 0.03$ Å has been used. Pair correlation functions have been used to investigate a detailed molecular structure for amorphous polymers [26–28]. Pair correlation functions have also been reported in the literature [41–43] in the characterization of liquid crystal structures by computer simulations.

Figures 14(*a*) and 14(*b*) depict the total pair correlation functions for MD121B in the SmE and SmA phases, respectively, as calculated by averaging ten equilibrated structures as a function of the distance r. These figures clearly indicate that similar pair correlation functions are obtained in the two phases. Also, the appearance of figures 14(*a*) and 14(*b*) is similar to that found in simulated systems of amorphous polymers, i.e. the total pair correlation functions exhibit no sign of order when the distance r is greater than 5 Å [26–28]. Peaks that appear as the result of intramolecular connections can be observed when the distance r is less than 5 Å. These peaks can be assigned by the length of chemical bonds. For example, the first two sharp peaks in figures 14(*a*)

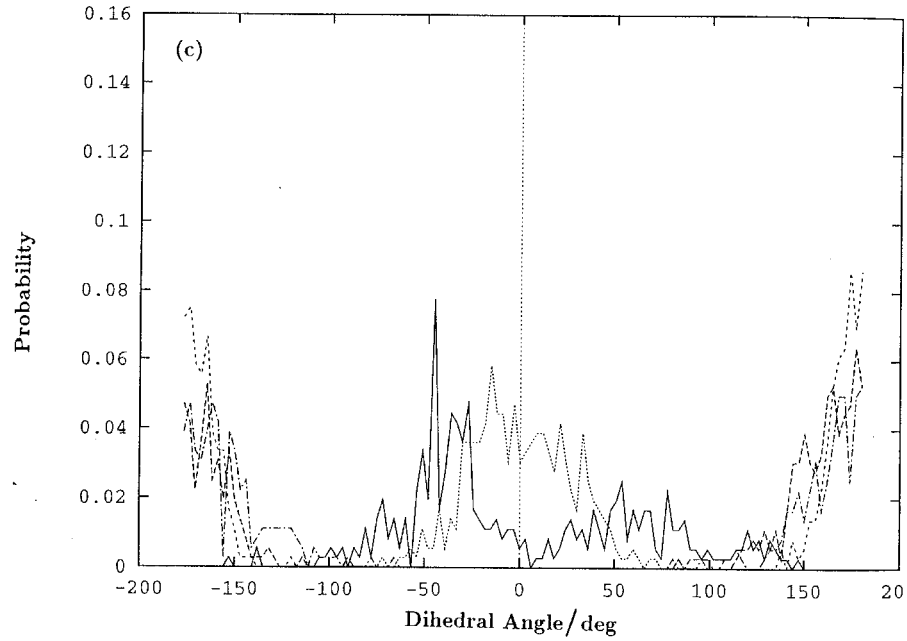

Figure 12. (*continued*).

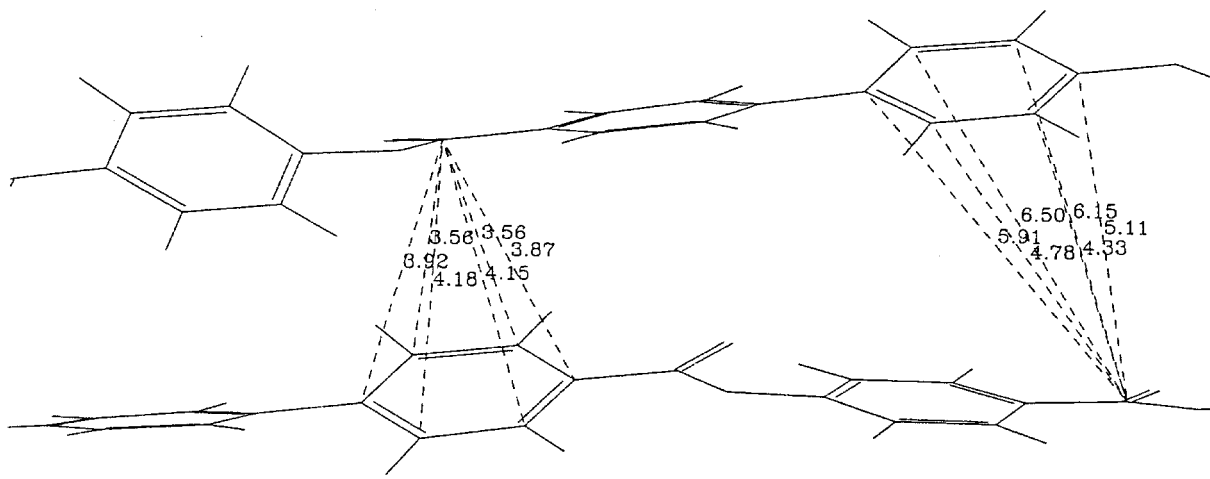

Figure 13. The aromatic core overlap. The dotted lines indicate the distances from the carbonyl groups at mesogen *i* to the aromatic rings at mesogen *j*.

and 14(*b*) originate from covalent bonds, and the next two peaks are derived from a pair of bonds. These peaks are C–H (1.07 Å), C–C (1.42 Å), H–C–C (2.17 Å), and C–C–C (2.43 Å); most of the contributions to the peaks due to C–C bonds arise from aromatic rings. As mentioned in the previous section, the most probable value of the range of the aromatic core overlap is ~5.2 Å. Beyond this distance, the structures of the simulated systems become random because distances between neighbouring atoms are not as fixed as those in local order. Therefore, no visible peaks appear beyond a distance of 5 Å in these figures.

4. Conclusions

In this study, the mesogenic molecules MD*n*21B studied experimentally in our previous work [16] have been simulated in the smectic E, A, and C phases with the aid of molecular modelling. This work has not only investigated the smectic phases on an atomistic level, but has also compared simulated and experimental X-ray diffraction patterns. A computer search with molecular mechanics calculations has made it possible to calculate intermolecular interaction energies and to find the favourable associations between two adjacent molecules. The lowest energy configurations of dimer associations

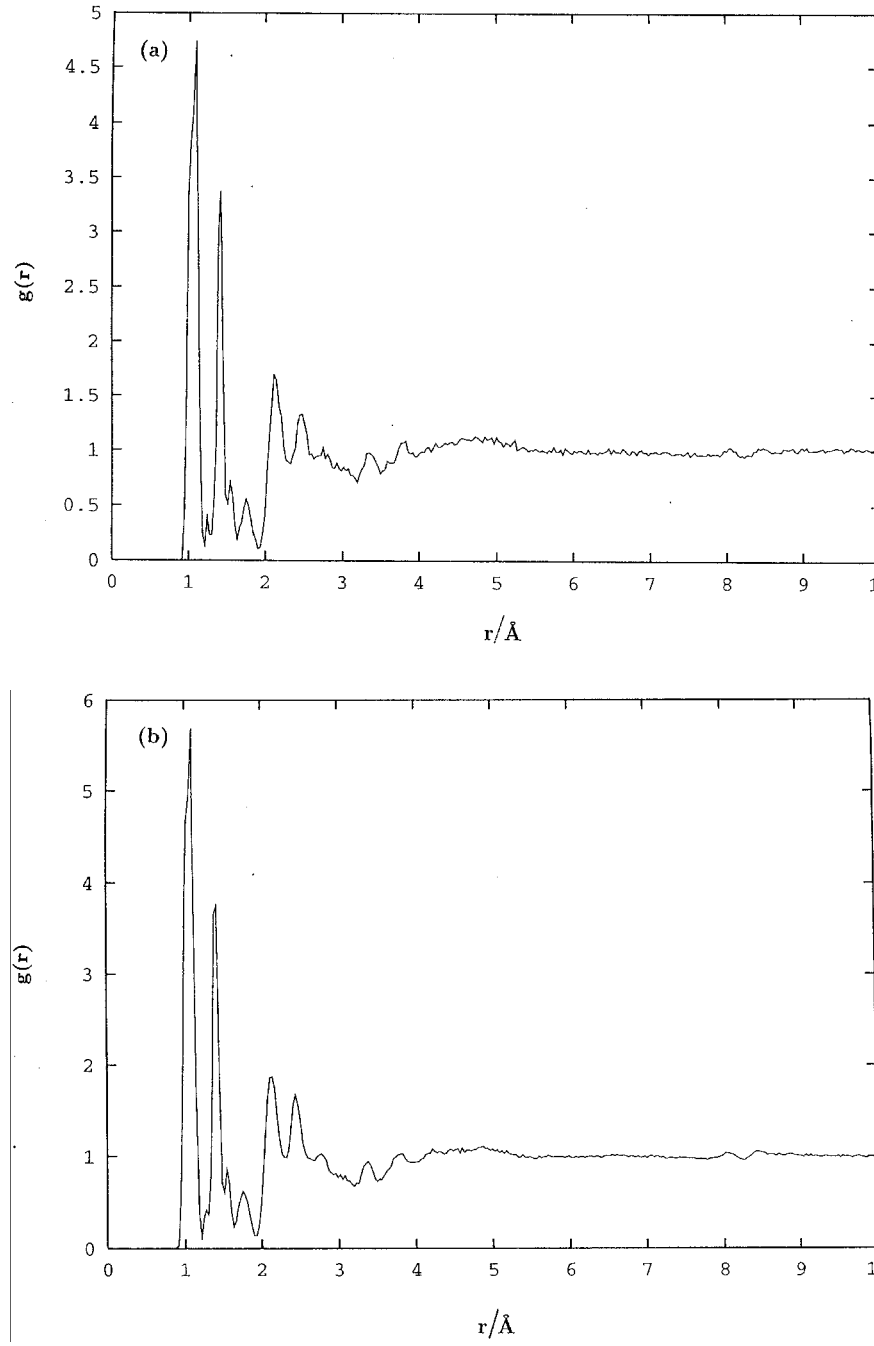

Figure 14. Total pair correlation function calculated for the equilibrated models of MD121B: (*a*) SmE phase, (*b*) SmA phase.

are antiparallel. Simulations of X-ray diffraction patterns have been conducted with the aid of Cerius[2], and the simulated models for the smectics E, A, and C are packed with antiparallel dimers, which have the lowest interaction energy. Ten starting models for each phase were constructed for these simulations. Simulation models for the SmE phase were constructed by following the work of Doucet and coworkers [22]. In addition, models for the SmA phase, having a liquid-like layer in two dimensions and a crystal order in one dimension, were also constructed. This liquid-like layer in the SmA phase could be obtained from molecular coordinates randomly transferred in two-dimensional directions on the basis of computer-generated random numbers. Moreover, models for the SmC phase were also developed in this manner by tilting the molecules in the SmA models with respect to the layer normal. These models achieve relaxation by combining energy minimizations and molecular dynamics runs under a canonical ensemble, and approach equilibrated states by performing further molecular

dynamics runs under an isobaric–isothermal ensemble. Simulations of X-ray diffraction patterns for smectics E, A, and C produced satisfactory agreements with those obtained experimentally.

The average values of aromatic core overlap are slightly higher than those of the lateral spacings, which were evaluated from the broad reflections of X-ray diffraction patterns at wide angles. However, the average values of aromatic core overlap for the SmA phase are close to the position $2\theta \sim 20^\circ$. This may support the fact that a broad X-ray reflection at wide angles associated with the average value of 4.5 Å, is constantly observed in the SmA phase.

The distributions of the dihedral angles at the bonds in the aromatic cores in the smectic phases indicate that there are two regions for the most probable appearance of the distributions. The distributions for ϕ_1 and ϕ_4 are around the *cis* conformation, and those for ϕ_2, ϕ_3, and ϕ_5 are centred at the *trans* conformation. Also, these distributions fluctuate around the values of the corresponding dihedral angles that were calculated with the aid of AM1 for the isolated molecule. Fluctuations of dihedral angles at the bonds in the aromatic cores in the SmA and SmC phases are higher than those in the SmE phase. This finding implies orientational disorder of the molecular long axis in the SmA and SmC phases, possibly causing a decrease in their *d* spacings.

The total pair correlation functions, as calculated for MD121B in the SmE and SmA phases, have a similar appearance, i.e. no visible peaks appear when the distance *r* is greater than 5 Å. This finding suggests that the most probable value of the range of aromatic core overlap is ~5.2 Å. These results may also suggest that in the smectic phases there is a local order in the range around 5 Å due to van der Waals interactions.

In general, molecular modelling may provide an alternative approach to a more thorough understanding of molecular configurations and arrangements in smectic phases.

The authors would like to thank the National Science Council of the Republic of China for financial support of this work under Contract No. NSC-84-2216-E007-029. This work was also financially supported by the National Centre for High-Performance Computing in Taiwan. K.-J. Lee thanks Dr M.-J. Hwang for providing the computer search algorithm.

References

[1] Gray, G. W., and Goodby, J. W., 1984, *Smectic Liquid Crystals: Textures and Structures* (Leonard-Hill).
[2] Blinov, L. M., and Chigrinov, V. G., 1994, *Electrooptic Effects in Liquid Crystal Materials* (Springer-Verlag).
[3] Meyer, R. B., Liebert, L., Strzelecki, L., and Keller, P., 1975, *J. Phys. Lett., Paris*, **36,** L69.
[4] Goodby, J. W., 1991, *Ferroelectric Liquid Crystals: Principles, Properties and Applications* (Gordon & Breach).
[5] Meyer, R. B., 1976, *Mol. cryst. liq. Cryst.*, **40,** 74.
[6] Garoff, S., and Meyer, R. B., 1977, *Phys. Rev. Lett.*, **38,** 848.
[7] Cladis, P. E., Bogardus, R. K., and Aadsen, D., 1978, *Phys. Rev. A*, **18,** 2292.
[8] Imrie, C. T., Schleeh, T., Karasz, F. E., and Attard, G. S., 1993, *Macromolecules*, **26,** 539.
[9] Dunmur, D. A., and Wilson, M. R., 1989, *Molecular Simulation*, **4,** 37.
[10] Wilson, M. R., and Dunmur, D. A., 1989, *Liq. Cryst.*, **5,** 987.
[11] Madhusudana, N. V., and Rajan, J., 1990, *Liq. Cryst.*, **7,** 31.
[12] Govind, A. S., and Madhusudana, N. V., 1993, *Liq. Cryst.*, **14,** 1539.
[13] Hsu, C.-S., Shih, L.-J., and Hsiue, G.-H., 1993, *Macromolecules*, **26,** 3161.
[14] Chen, J.-H., Chang, R.-C., Hsiue, G.-H., Guu, F.-W., and Wu, S.-L., 1995, *Liq. Cryst.*, **18,** 291.
[15] Hsiue, G.-H., and Chen, J.-H., 1995, *Macromolecules*, **28,** 4366.
[16] Hsiue, G.-H., Wu, J.-L., and Chen, J.-H., 1996, *Liq. Cryst.*, **21,** 449.
[17] Liang, C., Yan, L., Hill, J.-R., Ewig, C. S., Stouch, T. R., and Hagler, A. T., 1995, *J. comput. Chem.*, **16,** 883.
[18] Goldstein, H., 1950, *Classical Mechanics* (Addison Wesley).
[19] Mayo, S. L., Olafson, B. D., and Goddard, W. A., 1990, *J. phys. Chem.*, **94,** 8897.
[20] Rappé, A. K., and Goddard, W. A., 1991, *J. phys. Chem.*, **95,** 3358.
[21] Molecular Simulations, Inc., 9685 Scranton Road, San Diego, CA, USA.
[22] Doucet, J., Levelut, A. M., Lambert, M., Liebert, L., and Strzelecki, L., 1975, *J. Phys. (Paris) Colloq.*, **36,** C1–13.
[23] Pachter, R., Bunning, T. J., and Adams, W. W., 1991, *Comput. Polym. Sci.*, **1,** 179.
[24] Hofmann, D., Schneider, A. I., and Blackwell, J., 1994, *Polymer*, **35,** 5603.
[25] Ishaq, M., Blackwell, J., and Chvalun, S. N., 1996, *Polymer*, **37,** 1765.
[26] Fan, C. F., and Hsu, S. L., 1991, *Macromolecules*, **24,** 6244.
[27] Lee, K.-J., and Mattice, W. L., 1992, *Comput. Polym. Sci.*, **2,** 55.
[28] Zhang, R., and Mattice, W. L., 1995, *Macromolecules*, **28,** 7454.
[29] Nosé, S., 1984, *J. chem. Phys.*, **81,** 511.
[30] Nosé, S., 1984, *Mol. Phys.*, **52,** 255.
[31] Allen, M. P., and Tildesley, D. J., 1987, *Computer Simulation of Liquids* (Clarendon Press).
[32] Dewar, M. J. S., Zoebisch, E. G., Heary, E. F., and Stewart, J. J. P., 1985, *J. Am. chem. Soc.*, **107,** 3902.
[33] From the Quantum Chemistry Program Exchange (QCPE), Indiana University, Bloomington, IN, USA, Program 506.
[34] Hori, K., and Ohashi, Y., 1988, *Bull. chem. Soc. Jpn.*, **61,** 3859.
[35] Ito, K., Endo, K., and Hori, K., 1994, *Liq. Cryst.*, **17,** 747.

[36] KITANO, Y., USAMI, I., OBATA, Y., OKUYAMA, K., and JINDA, T., 1995, *Polymer*, **36,** 1123.
[37] ADAMS, J. M., and MORSI, S. E., 1976, *Acta crystallogr. (B)*, **32,** 1345.
[38] KAISER, J., RICHER, R., LEMKE, G., and GOLIC, L., 1980, *Acta crystallogr. (B)*, **36,** 193.
[39] AOTO, M., and OKAZAKI, K., 1993, *Ferroelectrics*, **148,** 51.
[40] KELLER, E. N., 1989, *Macromolecules*, **22,** 4597.
[41] AOKI, K. M., and YONEZAWA, F., 1993, *Liq. Cryst.*, **14,** 1237.
[42] WILSON, M. R., and ALLEN, M. P., 1993, *Mol. Phys.*, **80,** 277.
[43] LA PENNA, G., CATALANO, D., and VERACINI, C. A., 1996, *J. chem. Phys.*, **105,** 7097.